

MATHEMATICAL MODELLING OF ASPHALTENES DEPOSITION AND REMOVAL IN CRUDE DISTILLATION UNITS

D. Sileri, K. Sahu, H. Ding and O.K. Matar

Department of Chemical Engineering, Imperial College of London, SW7 2AZ London, UK.
dsileri@imperial.ac.uk

ABSTRACT

We have developed a mathematical model to describe quantitatively and qualitatively asphaltene deposition and removal in Crude Distillation Units pre-heat trains. The model is based on the conservation of mass, momentum and energy, including a chemical equilibrium model to account for phase separation and the deposition driven by thermal instability. We have performed numerical simulations to predict the rate of fouling, pressure drops and eventual removal rate via direct numerical simulations (DNS) and large eddy simulations (LES) using Diffuse Interface and Volume of Fluids methods, respectively. It is possible to account for aging of the foulant layer in time via an appropriate rheological model. The range of simulations spans from rectangular to cylindrical geometries and from laminar to turbulent flows. Further development will include a dependency on the composition of the oil used.

INTRODUCTION

Distillation processes of crude oil in a refinery account for a large portion of the energy needed for the entire process and in particular, fouling of pre-heat train exchangers (HXC) is responsible for reduced efficiency of the entire process and increased energy consumption. The high temperature the crude oil reaches inside those tube-shell heat exchangers destabilize some components in solution and triggers phase separation phenomena leading to fouling and worsening of hydraulic and thermal performances. The present work is part of a broader scheme, the CROF mainframe (Crude Oil Fouling <http://www3.imperial.ac.uk/crudeoilfouling>), which is working towards increasing the efficiency of the heat-recovery in the pre-heat train preventing and/or mitigating the formation of asphaltenes-based deposit (Venditti, Berruoco et al. 2009; Young, Venditti et al. 2009). The fouling of HXC is estimated to cost about 1.2 billions dollars and 7 millions tonnes of CO₂ emissions per year only in the US (ESDU 2005), nevertheless mechanism of deposition, removal and aging of the deposit are not yet fully understood. Currently, models for crude oil fouling are mostly based on empirical or semi-empirical correlations (TEMA 1988; Ebert and Panchal 1997), with little knowledge of the physics involved. It is therefore essential to accurately predict and understand the underlying

mechanisms. The aims of the present study are to develop capabilities to simulate accurately, reliably and efficiently the spatio-temporal evolution of the fouling process in the heat exchanger tubes as a function of the chemical, physical and thermal characteristics of the system. We adopted a new approach combining the mass momentum and energy conservation with a chemical equilibrium model based on the Gibbs free energy to account for the formation of the deposit and with a rheological model for the deposit to consider “aging-type” phenomena. The mathematical model obtain has been used to perform numerical simulation for both laminar and turbulent flows in different geometries. The predictions of the model are limited by the input into this model in terms of thermodynamic and physical properties. The reliability of the model predictions can therefore be enhanced with more accurate measurements of the latter, obtained in the other sub-projects of the CROF project (Hewitt, Macchietto et al. 2009).

PROBLEM FORMULATION

In our formulation we treat the oil and the deposit as fluids, considering the deposit prone to undergo aging to a hard material more similar to coke, difficult to remove by means of hydrodynamic forces. We then consider the flow of two immiscible, Newtonian and incompressible fluids of different density and viscosity in either a horizontal, planar channel or a cylindrical pipe and for both laminar and turbulent flows.

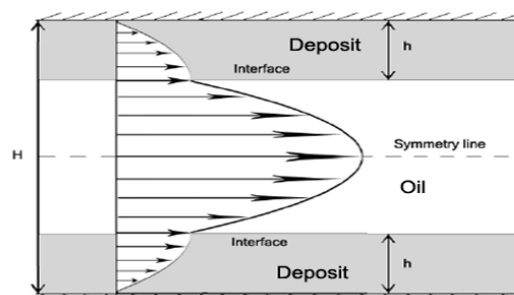


Figure 1: Schematic of the system

We focus on the displacement and removal of an initial layer of the more viscous fluid, referred to as the “deposit”, initially uniformly distributed at the walls of the domain.

The deposit is displaced by the less viscous fluid, referred to as the “oil”, by shear stresses and pressure at the interface between the two fluids.

Chemical Equilibrium Model

We complement the part relevant to the hydrodynamic and heat transfer with a chemical equilibrium model based on the Gibbs free energy (Won et al. 1986, Svendsen 1993). The model takes advantage of considering the oil as a multi-component mixture of hydrocarbons to quantify the amount of mass phase-separating in the oil and consequently diffusing and adhering to the walls. Assuming as an input the precipitation enthalpy, ΔH_{pi} , precipitation temperature, T_{pi} , and weight fraction for each component, the following expression is used to evaluate the equilibrium constant between the two phases for the oil mixture of n hydrocarbons:

$$K_i = \frac{d_i}{x_i} = K_{i0} \exp \left[-\frac{\Delta H_{pi}}{RT} \left(1 - \frac{T}{T_{pi}} \right) \right] \quad i = 1..,n \quad (1)$$

where d_i and x_i are the mole fractions of the “asphaltene-rich” phase and “oil-rich” phase for each component, respectively; T denotes the temperature of the oil-rich phase. To estimate the mass flux from the oil to the deposit we start from Fick’s law applied the asphaltene phase separated in the bulk and diffusing towards the wall:

$$J = D_d \frac{\partial \rho_d}{\partial n} \quad (2)$$

where D_d is the diffusion coefficient associated with the diffusing asphaltene species. By knowing that the asphaltene phase in the bulk is related to the oil density through its weight fraction:

$$\rho_d = \rho_o \chi_d \quad (3)$$

the flux J can then be re-expressed as:

$$J = D_d \left(\rho_o \frac{\partial \chi_d}{\partial n} \right) \quad (4)$$

which, after some manipulations, reads:

$$J = D_d \frac{\rho_o \eta}{T} \frac{\partial T}{\partial n} \quad (5)$$

where the dimensionless functions introduced have the form of:

$$\eta = \sum_{i=1}^n \eta_i \quad (6)$$

$$\eta_i = \chi_i \frac{\left[T(1+\mathcal{G})^2 \frac{\partial L_x}{\partial T} + \mathcal{G} \frac{\Delta H_{pi}}{RT} \right] K_i}{(1+\mathcal{G}K_i)^2} \quad (7)$$

Here, \mathcal{G} is a parameter that depends on the number of moles L_x present for each phase (Won et al. 1986, Svendsen 1993). Calculation of the temperature field in the oil-rich phase permits the calculation of the flux, J . For the present study, the oil is supposed to be characterized only by two components with characteristics listed table 1.

Table 1: Oil components properties

| Property | Value | Property | Value |
|-----------------|----------------|-----------------|-----------------|
| ΔH_{p1} | 34.9 kJ/mol | ΔH_{p2} | 107.8 kJ/mol |
| χ_1 | 0.96 | χ_2 | 0.04 |
| T_{p1} | 600 °K | T_{p2} | 423 °K |

Aging Model

From the literature and from collaboration with other CROF sub-projects (Saleh, Sheikholeslami et al. 2005; Hewitt, Macchietto et al. 2009; Tay and Kazarian 2009) we acknowledge that when the deposit adheres to the wall it experiences aging, when changes of properties in time are observed. In this case, a series of physico-chemical processes (coking) degrade the deposit to a hard material. We chose a rheological model for thixotropic materials developed by Coussot (Huynh, Roussel et al. 2005; Moller, Mewis et al. 2006; Coussot 2007) to characterize aging in the deposit. The apparent viscosity is the ratio between shear stress and shear rate:

$$\mu_d = \frac{\tau}{\dot{\gamma}} = \mu_0 (1 + \lambda^m) \quad (8)$$

where μ_0 and m are fluid parameters. The stress of the material depends on the local shear rate through a function depending on the state of structure. This state of structure is characterised by a variable λ , called the *structure parameter*, which describes the local degree of interconnection of the material microstructure and depends on flow history through a constitutive relation:

$$\frac{d\lambda}{dt} = \frac{1}{\theta} - \alpha \lambda \dot{\gamma} \quad (9)$$

The solution of the kinetic equation for λ Eq. (9) depends on the flow history and the rate of change of the structure parameter is the result of a competition between a “structuration” term, first term on the right hand side, and a “destructuration” term, second term on the right hand side. The structuration term depends on θ which is a

characteristic time for the formation of the microstructure while the destructure term depends on the local shear rate $\dot{\gamma}$, responsible for breaking down the formed microstructure, and on α which is a material-dependent constant.

We adopted two different approaches to solve the problem: direct numerical simulations for the laminar two-dimensional case and large eddy simulations for the turbulent three-dimensional case.

Direct Numerical Simulations

For the DNS simulations, we modified the original formulation of the Diffusive Interface Method (DIM) of Ding (Ding, Spelt et al. 2007; Sahu, Ding et al. 2009) to account for phase change and aging. We considered a two-dimensional, symmetric, horizontal channel where an initial uniform layer of viscous “deposit” is present at the walls and the less viscous “oil” flows from the left to the right. The inlet and outlet of the channel are placed at $x=0$ and $x=L$ of the horizontal direction, respectively. The walls are rigid and impermeable and are located at $z=0$ and $z=H$ in the vertical direction respectively. Hydrodynamic forces are responsible for the displacement of the deposit outside the channel whereas the phase-change in the bulk and the consequent deposition of material increase the mass of deposit with time following the formulation of the chemical equilibrium model. The deposit ages with time increasing gradually its viscosity and consequently inhibiting its removal from the channel depending on flow history and shear stresses as detailed in the aging model.

Governing equations

The conservation of mass, momentum, Chan-Hilliard (C-H) and energy equations are formulated as follows:

$$\nabla \cdot \mathbf{u} = 0 \quad (10)$$

$$\rho \left(\frac{\partial \mathbf{u}}{\partial t} + \mathbf{u} \cdot \nabla \mathbf{u} \right) = -\nabla p + \frac{1}{\text{Re}} \nabla \cdot \left[\mu (\nabla \mathbf{u} + \nabla \mathbf{u}^T) \right] + \frac{\phi \nabla C}{\text{Re} Ca} [1 - \beta(T-1)] \quad (11)$$

$$\frac{\partial C}{\partial t} + \mathbf{u} \cdot \nabla C = \frac{1}{Pe} \nabla \cdot (M \nabla \phi) + \frac{\eta}{D_s} \frac{(\mathbf{n} \cdot \nabla T)}{T} \quad (12)$$

$$\frac{\partial T}{\partial t} + \mathbf{u} \cdot \nabla T = \frac{1}{\text{Re} \text{Pr}} \nabla \cdot (\kappa \nabla T) \quad (13)$$

These dimensionless equations were obtained by scaling the equations using: the space H equal the height of the channel, the velocity V equal to the flow rate Q divided by H , the viscosity μ_0 , the density ρ_0 , the specific heat C_{p0} and the conductivity k_0 all properties of the bulk oil. For the

scaling of the Pe number in the CH equation we used the mobility parameter M and the chemical potential ϕ . For D_s has been used an opportune diffusion coefficient D . The complete set of equations can be found in (Ding, Spelt et al. 2007). With the respect to the original formulation, the last term in the RHS of Eq. (11) has been modified to include the surface tension and Marangoni effects. The last term in the RHS of Eq. (12) has been added to include deposition due to phase-change in the bulk accordingly with the chemical equilibrium model. Since the DIM formulation requires only one set of equations for the two phases, which is concentration-dependant, parameters such as density, viscosity and conductivity are themselves dependant on the concentration:

$$\rho / \rho_0 = C + (1 - C)r_d \quad (14)$$

$$\mu / \mu_0 = C + (1 - C)r_v \quad (15)$$

$$\kappa / \kappa_0 = C + (1 - C)r_k \quad (16)$$

Large Eddy Simulations

To perform LES studies we used a commercially-available software based on the Volume Of Fluids method: ANSYS-CFX (ANSYS 2006). We consider the flow of the two fluids in a cylindrical pipe, focussing on the displacement and removal of an initial layer of the more viscous fluid, referred to as the “deposit”, initially uniformly distributed at the wall of the pipe. The deposit is displaced by the less viscous fluid, referred to as the “oil”, by shear stresses and pressure at the interface between the two fluids. The inlet and outlet of the pipe are located at $x=0$ and $x=L$, respectively. The channel walls are rigid and impermeable and placed at distance r from the y axis. The flow is considered to be two-phase with the addition of a deposition mass-flux from the oil to the deposit driven by thermal instabilities and quantified by using a multi-component equilibrium model based on the Chemical Equilibrium Model

Governing equations

The conservation of mass, momentum and energy are solved for the entire domain and, to exploit the two-phase nature of the flow, an additional scalar variable called volume fraction C is introduced. The modified conservation equations are then modified as follows:

$$\frac{\partial \rho}{\partial t} + \nabla \cdot (\rho \mathbf{u}) = 0 \quad (17)$$

$$\frac{\partial(\rho \mathbf{u})}{\partial t} + \nabla \cdot (\rho \mathbf{u} \cdot \mathbf{u}) = -\nabla p + \nabla \cdot \left[\mu \left(\nabla \mathbf{u} + \nabla \mathbf{u}^T \right) \right] + S_M \quad (18)$$

$$\begin{aligned} \frac{\partial(C_\alpha \rho h_\alpha)}{\partial t} + \nabla \cdot [C_\alpha (\rho_\alpha \mathbf{u}_\alpha h_\alpha)] &= k_\alpha \nabla T_\alpha \\ + (\Gamma_{\alpha\beta}^+ h_{\beta\alpha} - \Gamma_{\beta\alpha}^+ h_{\alpha\beta}) + Q_\alpha + S_\alpha \end{aligned} \quad (19)$$

where the subscript α and β refer to the two fluids and where the second term in the RHS of Eq. (19) is related to the exchange of energy from the oil to the deposit due to the phase change. In this case the local density and viscosity are related to the volume fraction of the two fluids as follows:

$$\rho = \rho_\alpha C + \rho_\beta (1 - C) \quad (20)$$

$$\mu = \mu_\alpha C + \mu_\beta (1 - C) \quad (21)$$

The pipe walls are rigid and impermeable; moreover we also assume no-slip condition and constant temperature at the wall:

$$\mathbf{u} = 0 \text{ at wall}$$

$$T = T_w \text{ at wall}$$

We also assume constant flow rate at the inlet and constant pressure at the outlet.

The chosen model for turbulence LES resolves the largest and more energetic scales of flow motion associated with eddies and depending on the flow condition and geometry. The Navier-Stokes equations are then filtered and a sub-grid Scale model accounts for the smaller scale of turbulence of more general nature introducing an extra “eddy” viscosity.

For the numerical discretization we use a central difference scheme for the advection terms, a second order backward Euler scheme as a transient scheme.

RESULTS

DNS

Here, we focus on flows characterized by relatively low Reynolds numbers, which are reflective of those associated with pre-heat train exchanger. We have listed in Table 2 the dimensionless groups that parameterize the flow together with an order of magnitude estimate of their values.

We begin the presentation of our results by showing the outcome of our DNS simulations. Figure 2 depicts the volume fraction, temperature and viscosity fields at $t = 150$ for the parameter values listed in table 2 and the case of no-deposition and no-aging (obtained by setting $1/D_s$, $1/\theta$ and α to zero). It is seen that the deposit, which had formed at

earlier times along the domain (not shown), has been almost completely removed by the flow.

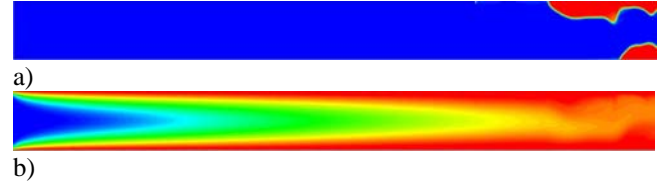


Figure 2: No-deposition and no-aging case: a) volume fraction, b) temperature. The parameter values are the same as those listed in table 1 and $1/D_s$, $1/\theta$ and α to zero. The blue color indicates the lowest value in the range whereas the red the highest.

Table 2: DNS simulations parameters

| Non dimensional parameter | Expression | Value |
|---------------------------|---|-----------|
| Re | $\frac{\rho_o V H}{\mu_o}$ | 500 |
| Pr | $\frac{C_{p,o} \mu_o}{\kappa_o}$ | 5.435 |
| Ca | $\frac{\mu_o V}{\sigma_o}$ | 0.00865 |
| Pe | $\frac{LV}{M\phi}$ | 1/EPS |
| Ds | $\frac{HV}{D}$ | 10^{12} |
| r_d | $\frac{\rho_d}{\rho_o}$ | 1.5 |
| r_c | $\frac{\kappa_d}{\kappa_o}$ | 10 |
| r_v | $\frac{\mu_0}{\mu_o}$ | 0.3 |
| β | $\frac{\partial \sigma_0 / \sigma_0}{\partial T}$ | 10 |

The next case considered corresponds to one involving no-aging but deposition through the phase-change effects evaluated with the chemical equilibrium model, which enter as a source term in the C-H equation. The deposition increases the mass of the deposit and competes with the removal by hydrodynamic forces, as shown in figure 3.

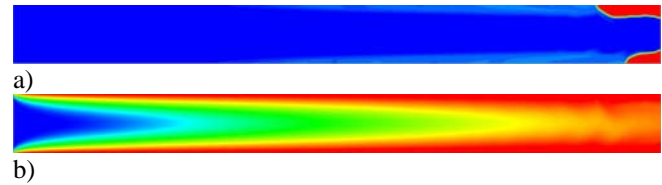


Figure 3: Deposition and no-aging case: a) volume fraction, b) temperature. The parameter values are the same as in figure 2 except for $D_s = 10^{12}$.

In the third case considered, aging was considered but deposition was not. As shown in Figure 4, it is evident that the removal of the deposit is slowed down by the increase in viscosity.

In Figure 5, we show the results associated with the case wherein both deposition and aging mechanisms are

considered. Here the average thickness and mass of the deposit increases with time due to deposition.

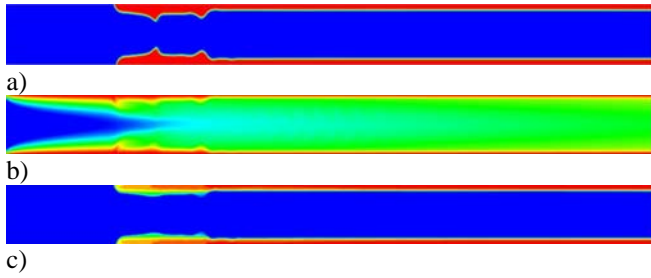


Figure 4: No-deposition/Aging case: a) volume fraction, b) temperature, c) viscosity. The parameter values are the same as in figure 2 except for $\theta=10$ and $\alpha=0.01$.

In addition, the increase in the viscosity of the deposit due to aging inhibits the development of instabilities that promote re-entrainment of the deposit in the bulk. This case therefore corresponds to the worst case scenario from a fouling perspective.

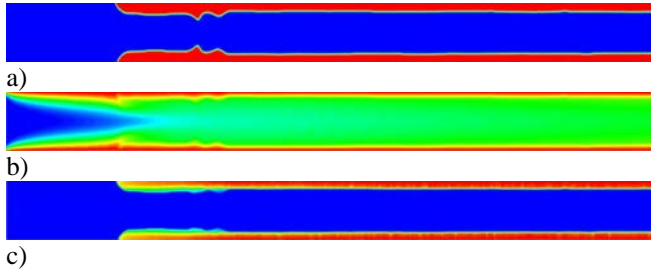


Figure 5: Deposition/Aging case: a) volume fraction, b) temperature, c) viscosity. The parameter values are the same as in figure 2 except for $Ds=10^{12}$, $\theta=10$ and $\alpha=0.01$.

In Figure 6, we plotted the mass of the deposit normalized by its initial mass over time for the four cases presented. For the parameter values used to generate this figure, it is clearly seen that the normalized deposit mass decreases to very small values in the absence of deposition and aging. For the cases where aging takes place, we see how the increase in viscosity ‘hardens’ the deposit with time making its removal very difficult. This is in qualitative agreement with experimental observations (Venditti, Berrueco et al. 2009).

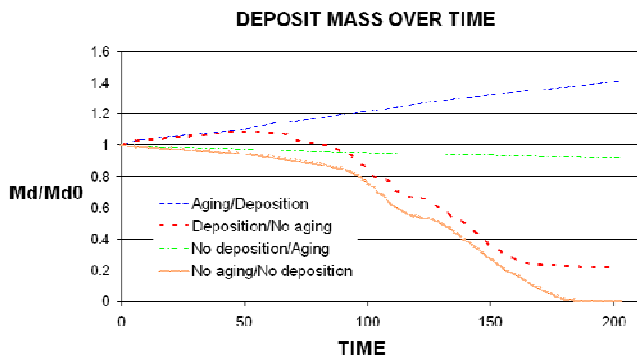


Figure 6: Deposit mass vs. time for the cases shown in figures 2-5.

LES

We present in Figure 7 the initial configuration of the domain used in the LES. In a) we show a plot of the mass fraction of the fluids where the red one is the initial deposit layer and the blue fluid is the oil flowing from left to right. In b) we have a projection of: the interface between the two fluids in green on the left; the mass of the deposit on the right in red. The complete list of geometry dimensions, flow conditions and fluid properties are in the table 3.

Table 3: LES simulations parameters

| | Units | Min | Max | Used |
|------------|----------------------|------|------|---------|
| ρ_o | [kg/m ³] | 600 | 900 | 7500 |
| ρ_d | [kg/m ³] | | | 1150 |
| μ_o | [kg/m s] | | | 0.00025 |
| μ_d | [kg/m s] | | | 0.05 |
| κ_o | [W/m.°C] | 0.1 | 0.13 | 0.115 |
| κ_d | [W/m.°C] | 0.2 | 2 | 1.1 |
| C_{Po} | [J/kg.°C] | 1500 | 3500 | 2500 |
| C_{Pd} | [J/kg.°C] | | | 2300 |
| σ_o | [mN/m] | | | 40 |
| L | [m] | | | 0.6 |
| V | [m/s] | | | 2 |
| H | [m] | | | 0.02 |
| T_w | [°K] | | | 573 |
| T_{in} | [°K] | | | 473 |

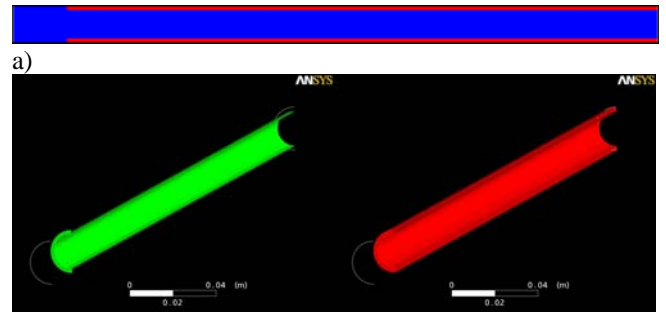


Figure 7: Initial configuration of a) volume fraction, b) interface and deposit mass for the LES.

We present two cases where the intensity of the deposition term differs and they are referred to as “J1” for small deposition and “J2” for the other. In Figure 8, we have a plot of the mass of the deposit in the vertical symmetry plane of the pipe at a later stage. We can observe in a) a much smaller quantity of deposit in comparison to b). This is due to a larger deposition contribution which enhances the amount of mass transferred from the oil to the deposit.

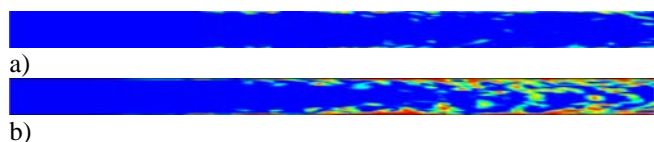


Figure 8: Volume fraction plot at time step=300 for a) J1 case, b) J2 case for the parameters shown in table 3.

The same situation is presented in Figure 9 where we show the total mass of deposit on the right side in red and the interface in green on the left. The highly turbulent nature of the flow in the bulk promotes the development of interfacial waves that lead to the detachment of portions of the deposit and their subsequent entrainment in the bulk and eventual from the pipe.

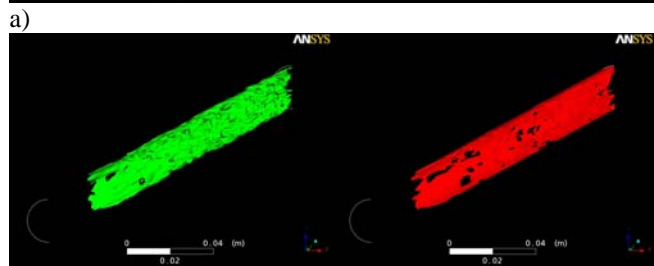
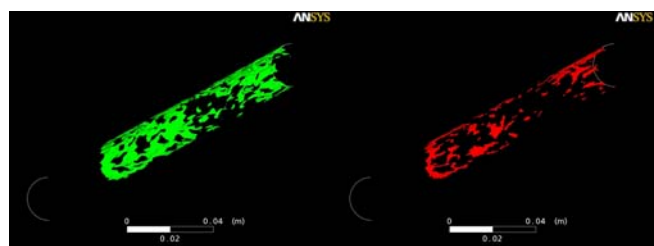


Figure 9: Interface and deposit mass at time step=300 for a) J1 case, b) J2 case, for the same parameters as in figure 8.

In Figure 10 we present a plot of mass versus time similar to the one presented for the DNS case, in the absence of aging. In agreement with the results presented in figure 6, when the physical properties of the deposit do not change in time due to aging effects, the removal of the deposit appears to be possible although further deposition of foulant material slows down the removal process. The case labeled 'J2' in figure 10 has a deposition term about five times larger than that associated with the 'J1' case. At $t = 300$, figure 10 shows that approximately 40% of the deposit remains; by comparison, in the J1 case the mass of deposit has decreased to zero over the same duration..

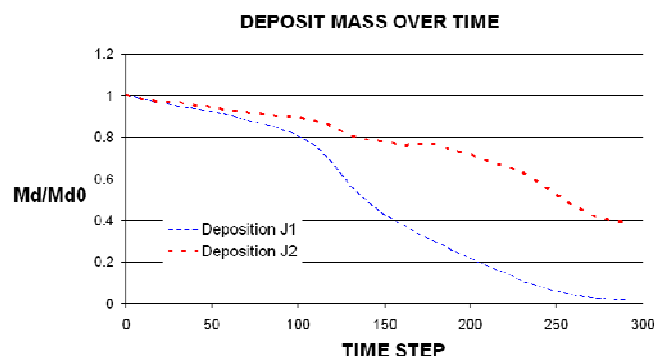


Figure 10: Deposit mass vs. time for the LES simulations whose results were presented in figures 8 and 9.

CONCLUSIONS

1. We have developed mathematical models that provide a quantitative description of fouling deposition and removal in pipes and channels.
2. The models account for the deposition of foulant material on the inside of conduits, their aging, and their removal through hydrodynamic interactions with the bulk phase.
3. The results of our direct numerical simulations and large eddy simulations indicate that the fouling problem is exacerbated by aging effects. Plots of the mass deposit with time show the possibility of complete deposit removal in the absence of aging; in the presence of these phenomena, our results indicate the gradual build-up of deposit thickness on the conduit walls. This may, ultimately, lead to blockage.

NOMENCLATURE

C concentration, dimensionless
 Ca capillary number,
 C_{p0} specific heat,
 d_i deposit mole fraction
 D_d deposit diffusion coefficient
 D_s inverse of diffusion coefficient
 EPS interface thickness, dimensionless
 h enthalpy
 H height of the channel/diameter of the pipe
 i index
 J deposition mass flux
 $J1$ deposition mass flux for LES case 1
 $J2$ deposition mass flux for LES case 2
 K_i equilibrium constant for component i
 K_{i0} equilibrium constant at precipitation temperature for component i
 L channel/pipe length
 L_x number of mole of "oil-rich" phase per mole mixture
 M mobility parameter
 \mathbf{n} normal vector
 m fluid parameter in the Aging Model
 p pressure
 Pe Peclet number
 Pr Prandtl number

Q interphase heat transfer
 r_d density ratio
 r_k conductivity ratio
 r_v viscosity ratio
 R gas constant
 Re Reynolds number
 S_M momentum source
 S external heat source
 t time
 T temperature
 T_{in} inlet temperature
 T_{pi} precipitation temperature for component i
 T_w constant wall temperature
 \mathbf{u} velocity vector
 u velocity
 V velocity
 x_i "oil-rich" mole fraction
 y cartesian coordinate

 β thermocapillarity term
 χ weight fraction
 ε material-dependent constant in the aging model
 ϕ chemical potential
 $\dot{\gamma}$ shear rate
 η dimensionless weight function
 κ thermal conductivity
 λ structure parameter
 μ viscosity
 ρ density
 σ surface tension
 τ shear stress
 ΔH_p precipitation enthalpy
 $\vartheta (1-L_x)/L_x$
 Γ mass flow rate

Subscript

i i -th component
 o oil
 d deposit
 0 initial
 x "oil-rich" phase
 α of phase alfa
 $\alpha\beta$ from phase alfa to phase beta
 $\beta\alpha$ from phase beta to phase alfa

REFERENCES

- ANSYS (2006). ANSYS CFX MANUAL Release 11.0. A. Inc.
- Coussot, P. (2007). "Rheophysics of pastes: a review of microscopic modelling approaches." Soft Matter **3**(5): 528-540.
- Ding, H., P. D. M. Spelt, et al. (2007). "Diffuse interface model for incompressible two-phase flows with large density ratios." Journal of Computational Physics **226**(2): 2078-2095.

- Ebert, W. A. and C. B. Panchal (1997). "Analysis of Exxon crude slip stream coking data." Fouling Mitigation of Industrial Heat-Exchange Equipment.
- ESDU (2005). Heat exchanger fouling in the pre-heat train of a crude oil distillation unit, ESDU.
- Hewitt, G. F., S. Macchietto, et al. (2009). Fouling in crude oil preheat trains: A systematic solution to an old problem. Heat Exchanger Fouling and Cleaning Schlading.
- Huynh, H. T., N. Roussel, et al. (2005). "Aging and free surface flow of a thixotropic fluid." Physics of Fluids **17**(3): -.
- Moller, P. C. F., J. Mewis, et al. (2006). "Yield stress and thixotropy: on the difficulty of measuring yield stresses in practice." Soft Matter **2**(4): 274-283.
- Sahu, K. C., H. Ding, et al. (2009). Pressure-driven miscible two-fluid channel flow with density gradients, AIP. **21**: 043603.
- Saleh, Z. S., R. Sheikholeslami, et al. (2005). "Fouling characteristics of a light Australian crude oil." Heat Transfer Engineering **26**(1): 15-22.
- Tay, F. h. and S. G. Kazarian (2009). Probing into Petroleum Heat-Exchanger Deposits using Attenuated Total Reflection Fourier-Transform Infrared Spectroscopic Imaging. Heat Exchanger Fouling and Cleaning. Schlading.
- TEMA (1988). Standards of the Tubular Exchanger Manufacturers Association, TEMA.
- Venditti, S., C. Berruoco, et al. (2009). Developing Characterisation Methods for Foulants Deposited in Refinery Heat Exchangers. Heat Exchanger Fouling and Cleaning. Schlading.
- Young, A., S. Venditti, et al. (2009). Characterization of Crude Oils and their Fouling Deposits. Heat Exchanger Fouling and Cleaning. Schlading.